Journal of Engineering Mathematics **28**: 345–364, 1994.

The three-dimensional boundary layer on a yawed body of revolution

T. ALLEN AND N. RILEY
School of Mathematics, University of East Anglia, Norwich, UK

Received 9 June 1993; accepted in revised version 30 October 1993

Abstract. A three-dimensional boundary layer calculation is carried out for the flow over a semi-infinite circular cylinder which is placed at a small angle of incidence to an oncoming uniform stream. To elucidate the details of the flow both a spectral and a finite difference method of solution has been employed. The results show that separation of 'open' type on a body of revolution is characterized by a line of Goldstein singularities that originates, spontaneously, at a finite distance from the nose of the body.

1. Introduction

In this paper we consider the three-dimensional boundary-layer flow over a semi-infinite circular cylinder that is placed at a small angle of incidence to a uniform stream. The small-incidence requirement allows a simple approximate form for the potential flow outside the boundary layer to be adopted.

It is well known that for two-dimensional flow, the boundary-layer equations exhibit singular behaviour at a point of zero skin-friction. This singular behaviour was first analysed by Goldstein [1], by whose name it is commonly called, and completed by Stewartson [2]. Numerical studies, by Terrill [3] in particular, have confirmed all essential features of the Goldstein singularity which is accepted as a mathematical manifestation of the large changes that take place in the flow at separation. The role of classical boundary-layer theory within the framework of high-Reynolds number flows has been elucidated by interaction theories, of which a local notable theory is the now classical 'triple deck' (see, e.g., Stewartson [4], Smith [5]). Boundary-layer separation in three dimensions is perhaps less well understood, and one of the main aims herein is to illuminate certain aspects of so-called 'open' separation.

Sufficiently far along the cylinder the flow may be expected to be largely independent of features in the neighbourhood of the nose of the cylinder, and distance measured along it. That being so, the equations decouple and the flow perpendicular to the generators of the cylinder will terminate in singular behaviour of the Goldstein type. Two questions arise. The first is 'what is the extent of the region of flow which is largely independent of the streamwise coordinate?'. The second, related and perhaps more fundamental question, is 'does the singularity in the solution which is expected far downstream emerge only in the asymptotic limit, or does it appear spontaneously at a finite distance from the cylinder nose?'. There is already evidence in favour of the latter scenario. First, note that Brown [6] has shown that in conefield flow the solution at a separation line may exhibit singular behaviour along its entire length from the apex. The numerical investigation carried out by Cooke [7] confirms that singular behaviour of Goldstein type does indeed occur. Second, there is the analogy between the problem under consideration and the unsteady two-dimensional situation of an

infinite cylinder moved impulsively perpendicular to its generators. Lighthill [8] has highlighted this analogy. He argues that as fluid is convected past the cylinder with free-stream speed U_∞ the position of the cylinder appears to change at a rate $U_\infty \sin \alpha$, where α is the incidence. The fluid may therefore develop a boundary layer, with an axial component of vorticity, which grows causing flow separation, identified as cross-stream flow reversal, first at the leeward generator and then further forward. Ultimately, the growing wake becomes unstable and sheds vorticity. If the convective velocity along the cylinder within the boundary layer were constant, which it cannot be since the no-slip condition must be satisfied, then the analogy would be exact. The work of van Dommelen and Shen [9], and Cowley [10] shows that for the unsteady two-dimensional problem the solution fails, in a singular fashion, at a finite time. An exact analogy would therefore require the steady three-dimensional boundary-layer solution to fail, similarly, at a finite distance from the nose. Although, as we have indicated, the analogy is by no means exact our numerical solution does exhibit a spontaneous eruptive singularity at a finite distance from the nose. The structure of this singularity, as may be expected, is different from that in the unsteady two-dimensional flow although we have been unable to provide a complete analysis of it. Downstream from this initial singular point trails a line of singularities, of Goldstein type, which is almost coincident with a cylinder generator. It is shown that this approaches the position of two-dimensional separation far downstream.

The equations governing our three-dimensional boundary-layer flow are set out in Section 2, and in Section 3 we examine by partly analytic, and partly numerical means the flow along the windward and leeward generators of the cylinder. The solution along the leeward generator, in particular, reinforces the analogue idea between steady three-dimensional and unsteady two-dimensional boundary-layer flows. The techniques adopted for the solution of the three-dimensional boundary-layer flow are set out in Section 4. Two methods are described there, one is a spectral method, the other a finite-difference method. Each has its use, as explained, and both have been used, in different parts of the flowfield to build up the picture of the flow properties that are described in Section 5. The results we have obtained enable us to comment upon the independence principle. But our main conclusion is that flow separation of the 'open' type on a body of revolution is characterized, in a three-dimensional boundary-layer calculation by a line of singularities which commences spontaneously at a finite distance from the nose of the body.

2. Problem definition and governing equations

We are concerned with the three-dimensional boundary layer that forms on a semi-infinite circular cylinder of radius a whose generators are inclined at a small angle ε to a uniform stream of speed U_∞. With reference to the definition sketch, Fig. 1, dimensionless cylindrical polar coordinates (r, θ, z) are introduced, where a has been chosen as a typical length scale. For the potential flow outside the boundary layer we take as the velocity potential

$$\phi = z - \varepsilon\left(r + \frac{1}{r}\right)\cos\theta \,, \tag{1}$$

where aU_∞ has been taken as the scale for ϕ. This simple potential cannot describe the complex three-dimensional flow in the nose-region of the cylinder, but it will be an

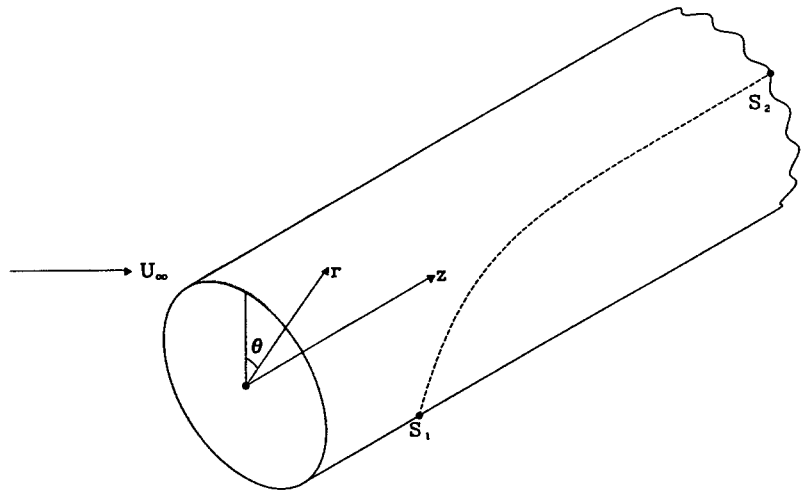

Fig. 1. Definition sketch. The line S_1S_2 is the line on which $\partial v/\partial y|_{y=0}$ changes sign.

appropriate representation, for $\varepsilon \ll 1$, of the flow at large distances downstream, where our major interests lie. If (U, V, W) are the dimensional velocity components in the cylindrical polar coordinate system then we make these dimensionless by writing $U = U_\infty u$, $V = \varepsilon U_\infty v$, $W = R_e^{-1/2} U_\infty w^*$ where $R_e = aU_\infty/\nu$ is the Reynolds number. The boundary-layer equations for the flow at the cylinder surface are, then, in the high-Reynolds number limit and with $r = 1 + R_e^{-1/2}\bar{y}$,

$$
\begin{aligned}
&u\frac{\partial u}{\partial z} + \varepsilon v\frac{\partial u}{\partial \theta} + w^*\frac{\partial u}{\partial \bar{y}} = \frac{\partial^2 u}{\partial \bar{y}^2}\,,\\
&u\frac{\partial v}{\partial z} + \varepsilon v\frac{\partial v}{\partial \theta} + w^*\frac{\partial v}{\partial \bar{y}} = 2\varepsilon \sin 2\theta + \frac{\partial^2 v}{\partial \bar{y}^2}\,,\\
&\frac{\partial u}{\partial z} + \varepsilon\frac{\partial v}{\partial \theta} + \frac{\partial w^*}{\partial \bar{y}} = 0\,.
\end{aligned}
\tag{2}
$$

It is convenient to formally eliminate ε from equations (2) by writing $z = x/\varepsilon$, $\bar{y} = y/\sqrt{\varepsilon}$, $w^* = \sqrt{\varepsilon}\bar{w}$, so that we have

$$
\begin{aligned}
&u\frac{\partial u}{\partial x} + v\frac{\partial u}{\partial \theta} + \bar{w}\frac{\partial u}{\partial y} = \frac{\partial^2 u}{\partial y^2}\,,\\
&u\frac{\partial v}{\partial x} + v\frac{\partial v}{\partial \theta} + \bar{w}\frac{\partial v}{\partial y} = 2\sin 2\theta + \frac{\partial^2 v}{\partial y^2}\,,\\
&\frac{\partial u}{\partial x} + \frac{\partial v}{\partial \theta} + \frac{\partial \bar{w}}{\partial y} = 0\,,
\end{aligned}
\tag{3}
$$

as our governing equations. The boundary conditions for equations (3) require

$$
u = v = \bar{w} = 0 \quad \text{on} \quad y = 0\,, \tag{4}
$$

and

$$u \to 1, v \to 2\sin\theta \quad \text{as} \quad y \to \infty .$$

In addition to the conditions (4), conditions at some initial station are required. This we take to be $x = 0$ where the boundary layer is assumed to grow in the manner of the Blasius boundary layer on a flat plate. Whilst this might be difficult to realise in practice, it does, along with the potential (1), serve our purposes in the sense that flow conditions far downstream will be largely unaffected by those in the nose-region of the cylinder. The solution for u as $x \to 0$ will be $u = u_b(\eta)$ where $\eta = y/\sqrt{x}$. This prompts a change of variables from (x, θ, y) to (x, θ, η) so that equations (3) now become, with $w = \sqrt{x}\bar{w}$,

$$\begin{aligned}
&xu\frac{\partial u}{\partial x} + xv\frac{\partial u}{\partial \theta} + (w - \tfrac{1}{2}\eta u)\frac{\partial u}{\partial \eta} = \frac{\partial^2 u}{\partial \eta^2}, \\
&xu\frac{\partial v}{\partial x} + xv\frac{\partial v}{\partial \theta} + (w - \tfrac{1}{2}\eta u)\frac{\partial v}{\partial \eta} = 2x\sin 2\theta + \frac{\partial^2 v}{\partial \eta^2}, \\
&x\frac{\partial u}{\partial x} + x\frac{\partial v}{\partial \theta} + \frac{\partial w}{\partial \eta} - \tfrac{1}{2}\eta\frac{\partial u}{\partial \eta} = 0 .
\end{aligned} \tag{5}$$

The boundary conditions (4) now become

$$\begin{aligned}
&u = v = w = 0 \qquad \text{on} \quad \eta = 0, \quad \forall x > 0, \\
&u \to 1, v \to 2\sin\theta \quad \text{as} \quad \eta \to \infty, \quad \forall x > 0,
\end{aligned} \tag{6}$$

with

$$u = u_b(\eta) \quad \text{at} \quad x = 0 ,$$

where u_b is determined, by setting $x \equiv 0$ in $(5)_{1,3}$, from

$$-\tfrac{1}{2}\eta u_b u_b' + w_b u_b' = u_b'', \qquad -\tfrac{1}{2}\eta u_b' + w_b' = 0 , \tag{7}$$

with

$$u_b = w_b = 0 \quad \text{on} \quad \eta = 0, \qquad u_b \to 1 \quad \text{as} \, \eta \to \infty ,$$

and a prime denotes differentiation with respect to η. The remaining boundary condition, on v at $x = 0$, is obtained by setting $x = 0$ in $(5)_2$. Inspection shows that $v \propto u_b$, and the condition (6) as $\eta \to \infty$ gives

$$v = 2u_b(\eta)\sin\theta \quad \text{at} \, x = 0 . \tag{8}$$

The equations (5), (6) and (8) are the forms of the governing equations that we have used for numerical solution. Two numerical schemes have been adopted, one is a spectral method the other a finite-difference method. Before describing these in detail, and the results derived therefrom, we consider the flow conditions at the two generators which correspond to the windward and leeward stagnation lines of the outer, inviscid flow.

3. Flow conditions at $\theta = 0, \pi$

Consider first the windward generator $\theta = 0$. For large x flow conditions may be expected to become independent of x. Setting $\partial/\partial x \equiv 0$ in equations (3) and expanding, close to $\theta = 0$,

$$u = g(\zeta) + O(\theta^2), \qquad v = 2\theta f'(\zeta) + O(\theta^3), \qquad \bar{w} = -\sqrt{2} f(\zeta) + O(\theta^2), \tag{9}$$

where $\zeta = \sqrt{2}y$, then the reduced form of $(3)_3$ is satisfied identically at leading order, whilst $(3)_2$ and $(3)_1$ give, at leading order, respectively

$$\begin{aligned} &f''' + ff'' - f'^2 + 1 = 0, \qquad && f(0) = f'(0) = 0,\ f'(\infty) = 1, \\ &g'' + fg' = 0, && g(0) = 0,\ g(\infty) = 1, \end{aligned} \tag{10}$$

where a prime denotes differentiation with respect to ζ. These are the equations appropriate to the stagnation line of attachment on an infinite yawed cylinder and, indeed, that for f is simply the equation for two-dimensional stagnation point flow.

We may infer that ultimately, for large x, flow conditions along the line of attachment become independent of the coordinate x. The same is not true at the leeward stagnation line however, where the flow has much in common with the flow at the rear stagnation point of an impulsively moved cylinder in two dimensions. Suppose that close to the leeward generator $\theta = \pi$ we write

$$\begin{aligned} &u = u_l(x, y) + O(\pi - \theta)^2, \qquad v = (\pi - \theta) v_l(x, y) + O(\pi - \theta)^3, \\ &\bar{w} = w_l(x, y) + O(\pi - \theta)^2, \end{aligned} \tag{11}$$

then, at leading order, equations (3) give

$$\begin{aligned} &u_l \frac{\partial u_l}{\partial x} + w_l \frac{\partial u_l}{\partial y} = \frac{\partial^2 u_l}{\partial y^2}, \\ &u_l \frac{\partial v_l}{\partial x} - v_l^2 + w_l \frac{\partial v_l}{\partial y} = \frac{\partial^2 v_l}{\partial y^2} - 4, \\ &\frac{\partial u_l}{\partial x} - v_l + \frac{\partial w_l}{\partial y} = 0. \end{aligned} \tag{12}$$

If we proceed as at the stagnation line of attachment, and set $\partial/\partial x \equiv 0$, then $(12)_{2,3}$ are the equations for two-dimensional rear stagnation point flow for which there is no solution. Guided by the work of Proudman and Johnson [11] for the unsteady two-dimensional problem we may suppose that in the present case the flow at the rear stagnation line divides into an inner viscous layer and an outer region of inviscid, rotational flow as $x \to \infty$. For the outer layer we introduce a new coordinate $\xi = y\, e^{-\lambda x}$, where λ is a constant, and variables $w_0 = w_l\, e^{-\lambda x}$, $v_0 = v_l$, $u_0 = u_l$ so that as $x \to \infty$ equations (12) become

$$\begin{aligned} &(w_0 - \lambda \xi u_0) \frac{\partial u_0}{\partial \xi} = 0, \\ &(w_0 - \lambda \xi u_0) \frac{\partial v_0}{\partial \xi} - v_0^2 = -4, \\ &-\lambda \xi \frac{\partial u_0}{\partial \xi} - v_0 + \frac{\partial w_0}{\partial \xi} = 0. \end{aligned} \tag{13}$$

If $\partial u_0/\partial \xi \neq 0$ then $(13)_1$ gives $w_0 = \lambda \xi u_0$ and $(13)_2$ then gives $v_0 = 2$, so that finally from $(13)_3$ $u_0 = 2/\lambda$ which determines $\lambda = 2$ if the solutions are to match with the outer potential flow. With $u_0 \equiv 1$ our procedure is inconsistent and all we have done is recover the outer

irrotational flow solution close to the boundary. If $\partial u_0/\partial\xi = 0$, so that $u_0 \equiv 1$, equation $(13)_1$ is satisfied and writing $v_0 = f_0'(\xi)$, $w_0 = f_0(\xi)$, where a prime now denotes differentiation with respect to ξ, equation $(13)_3$ is satisfied identically whilst $(13)_2$ requires

$$-\lambda\xi f_0'' - f_0'^2 + f_0 f_0'' = 4\,. \tag{14}$$

The solution of (14) which satisfies $f_0(0) = 0$, and decays exponentially as $\xi \to \infty$, is

$$f_0 = 2\xi - \frac{4}{c}(1 - \mathrm{e}^{-c\xi})\,, \tag{15}$$

where c is an undetermined constant. Note now, from (12) and (15), that as $y \to 0$,

$$u_l \to 1, v_l \to -2(\pi - \theta)\,, \tag{16}$$

which means that the inner viscous layer that is required to satisfy the no-slip condition is identical in structure with that at the windward stagnation line.

In order to test the form of solution for large x, on both the windward and leeward stagnation lines, equations (5) have been integrated along each of these lines, with a factor of θ or $\pi - \theta$ removed from v as appropriate, using a finite-difference method adapted from that described below for the three-dimensional calculation. The results are shown in Fig. 2. We note how rapidly $\theta^{-1}\,\partial v/\partial y|_{y=0}$ and $\partial u/\partial y|_{y=0}$ approach constant values on the windward stagnation line. By contrast the corresponding quantities on the leeward stagnation line, namely $(\pi - \theta)^{-1}\,\partial v/\partial y|_{y=0}$ and $\partial u/\partial y|_{y=0}$, approach their terminal values more slowly but they do, as predicted above, approach the same values as for the windward stagnation line. The particular quantities shown in Fig. 2 might suggest that sufficiently far from the nose of the cylinder flow properties are becoming independent of the coordinate x. Such a conclusion is, however, misleading since as we have seen above, the viscous layer on the leeward stagnation line is embedded within a region of inviscid rotational flow whose

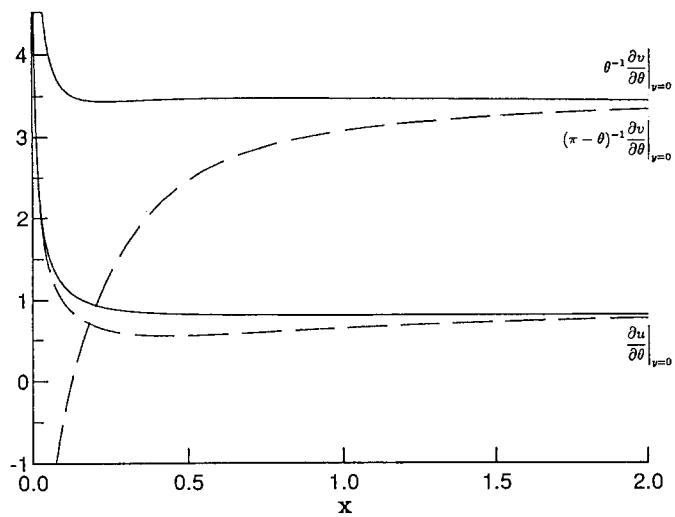

Fig. 2. Variation with x of $\partial u/\partial y$ and $\theta^{-1}\,\partial v/\partial y$ (windward) or $(\pi - \theta)^{-1}\,\partial v/\partial y$ (leeward) at $y = 0$ on the windward ———, and the ——— leeward, generators.

thickness is increasing dramatically as x increases. We shall return to the dependence of flow features upon x in our discussion below on the results of our three-dimensional calculations.

4. Numerical methods

To solve equations (5) subject to the conditions (6) and (8) we have adopted two methods, namely a finite-difference method and a spectral method. Each has a role to play, as we shall indicate, and each is described separately below.

4.1. Finite-difference method

In essence, our finite-difference method integrates equations (5) along the generators of the cylinder, from some initial station x_0, starting with the windward generator $\theta = 0$ and at the end of each x-sweep advancing to a neighbouring generator in increments of $\delta\theta$. If the integration commences at $x = 0$ then the Blasius solution of the ordinary differential equations (7) is required.

In order to implement the scheme outlined above we must first establish the solution on $\theta = 0$. To enable this write

$$u = \bar{u}(x, \eta) + O(\theta^2), \qquad v = \theta\bar{v}(x, \eta) + O(\theta^3), \qquad w = \bar{w}(x, \eta) + O(\theta^2), \tag{17}$$

to give, upon substitution into (5), for the leading terms

$$\begin{aligned} &x\bar{u}\frac{\partial\bar{u}}{\partial x} + (\bar{w} - \tfrac{1}{2}\eta\bar{u})\frac{\partial\bar{u}}{\partial\eta} = \frac{\partial^2\bar{u}}{\partial\eta^2}, \\ &x\bar{u}\frac{\partial\bar{v}}{\partial x} + x\bar{v}^2 + (\bar{w} - \tfrac{1}{2}\eta\bar{u})\frac{\partial\bar{v}}{\partial\eta} = 4x + \frac{\partial^2\bar{v}}{\partial\eta^2}, \\ &x\frac{\partial\bar{u}}{\partial x} + x\bar{v} + \frac{\partial\bar{w}}{\partial\eta} - \tfrac{1}{2}\eta\frac{\partial\bar{u}}{\partial\eta} = 0. \end{aligned} \tag{18}$$

We remark that it is these equations, and a companion set appropriate to $\theta = \pi$, that have been integrated to obtain the results shown in Fig. 2. The finite-difference representation of (18) which is adopted employs backward differences in x and central differences in η. With reference to Fig. 3 the point (i, j) refers to the point whose coordinates are $\{(i-1)\,\delta x, (j-1)\,\delta\eta\}$; and we adopt a standard suffix notation such that $\bar{u}_{i,j}$ represents the value of $\bar{u}$ at that point. The set of equations (18) is solved iteratively and quasi-linearization must be employed so that, for example, the term $\bar{u}\,\partial\bar{u}/\partial x$ is written as

$$\bar{u}\frac{\partial\bar{u}}{\partial x} = \tilde{\bar{u}}\frac{\partial\bar{u}}{\partial x} + \bar{u}\frac{\partial\tilde{\bar{u}}}{\partial x} - \tilde{\bar{u}}\frac{\partial\tilde{\bar{u}}}{\partial x}, \tag{19}$$

where a tilde denotes the value of $\bar{u}$ from a previous iterate. The terms $\bar{u}\,\partial\bar{u}/\partial\eta$ and $\bar{v}^2$ are similarly quasi-linearized. In the finite-difference representations the quasi-linearized form of equations $(18)_{1,2}$ are evaluated at $(i+1, j)$, denoted by ○ in Fig. 3, whilst $(18)_3$ is evaluated at $(i+1, j-\frac{1}{2})$, denoted by × in Fig. 3. The finite-difference representations of (18) may then be written as

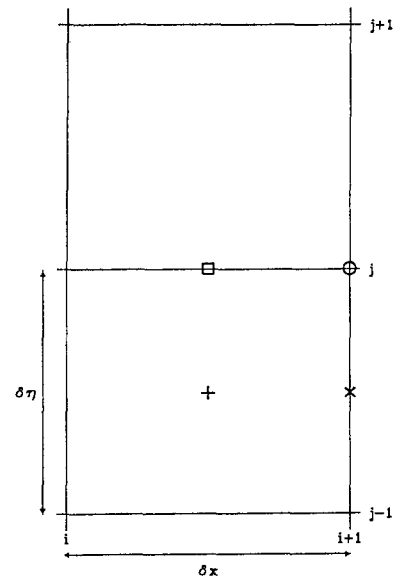

Fig. 3. The computational mesh for the calculation of the initial solution along the windward generator.

$$\begin{aligned}
&\bar{a}_j\bar{u}_{i+1,j+1} + \bar{b}_j\bar{u}_{i+1,j} + \bar{c}_j\bar{u}_{i+1,j-1} = \bar{d}_j\,,\\
&\bar{A}_j\bar{v}_{i+1,j+1} + \bar{B}_j\bar{v}_{i+1,j} + \bar{C}_j\bar{v}_{i+1,j-1} = \bar{D}_j\,,\\
&\bar{w}_{i+1,j} - \bar{w}_{i+1,j-1} = \bar{e}_j\,,
\end{aligned} \tag{20}$$

where $j = 2$ to $n-1$, so that the assumed outer edge of the boundary layer is $\eta_\infty = (n-1)\,\delta\eta$.

The solution strategy we have adopted to advance from station i to station $i+1$ is as follows. Estimates of $\bar{u}$, $\bar{v}$ at $i+1$ are made by extrapolation from the solution at previous stations. From these a first estimate of $\bar{w}$ is made from $(20)_3$. Equation $(20)_1$, which is the finite-difference representation of the quasi-linearized form of $(18)_1$, is then solved iteratively to obtain a partially converged update of $\bar{u}$; a partially converged update of $\bar{v}$ is then obtained by similarly solving $(18)_2$ in an iterative manner. Equation $(18)_3$ then gives a new estimate of $\bar{w}$ and the whole process is repeated until converged values of $\bar{u}$, $\bar{v}$ and $\bar{w}$ are obtained according to some pre-set criterion.

With the solution along the generator $\theta = 0$ determined, as described above, we can now advance to the next generator $\theta = \delta\theta$, and integrate equations (5) along it. Quasi-linearization, as in (19) is again employed, and the finite-difference representation again uses central differences in η, with backward differences in θ and x. Thus, the quasi-linearized forms of $(5)_{1,2}$ are evaluated at $(i+1, j, k+1)$, denoted by ○ in Fig. 4, whilst $(5)_3$ is evaluated at $(i+1, j-\frac{1}{2}, k+1)$, denoted by × in Fig. 4. The finite-difference representations of (5) may be written, in a similar manner to (20), as

$$\begin{aligned}
&a_j u_{i+1,j+1,k+1} + b_j u_{i+1,j,k+1} + c_j u_{i+1,j-1,k+1} = d_j\,,\\
&A_j v_{i+1,j+1,k+1} + B_j v_{i+1,j,k+1} + C_j v_{i+1,j-1,k+1} = D_j\,,\\
&w_{i+1,j,k+1} - w_{i+1,j-1,k+1} = e_j\,,
\end{aligned} \tag{21}$$

where again $j = 2$ to $n-1$. The solution strategy is as for equations (20), with initial estimates for u, v at $(i+1, j, k+1)$ being given from the previously determined values at (i, j, k), $(i+1, j, k)$, $(i, j, k+1)$. For each of the sets of equations $(20)_{1,2}$, $(21)_{1,2}$ advantage is taken of the tridiagonal structure of the matrix of coefficients via the Thomas algorithm.

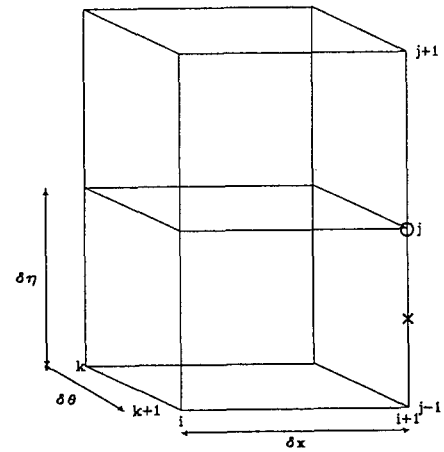

Fig. 4. The computational mesh for the three dimensional calculation.

The finite-difference method described above does not allow us to compute the boundary layer over the whole of the cylinder surface for the following reason. Consider, in Fig. 1, the line S_1S_2. If this line is denoted by $\theta = \theta_l(x)$ then for $\theta < \theta_l$, $\partial v/\partial\eta|_{\eta=0} > 0$, whilst for $\theta > \theta_l$, $\partial v/\partial\eta|_{\eta=0} < 0$. The onset of this line at the point S_1 can be seen in Fig. 2. This is the point at which $(\pi - \theta)^{-1}\, \partial v/\partial y|_{y=0}$ changes sign in that figure. This change of sign in the azimuthal shear stress component implies a reversed flow close to the boundary for $\theta > \theta_l$ which, in turn, means that in any satisfactory computational scheme conditions on the leeward generator cannot be ignored. It is, therefore, not surprising that our finite-difference scheme, as outlined above, fails to penetrate this region of reversed flow. More complex finite-difference schemes may be constructed, but to overcome this particular difficulty we have adopted a spectral method described in the next sub-section.

4.2. Spectral method

To take account of conditions on $\theta = 0,\ \pi$ the components u, w are expanded as even functions of θ, and v as an odd function of θ, so that

$$\begin{aligned} u(x,\eta,\theta) &= u_0(x,\eta) + \sum_{n=1}^{\infty} u_n(x,\eta)\cos n\theta\ , \\ v(x,\eta,\theta) &= \sum_{n=1}^{\infty} v_n(x,\eta)\sin n\theta\ , \\ w(x,\eta,\theta) &= w_0(x,\eta) + \sum_{n=1}^{\infty} w_n(x,\eta)\cos n\theta\ . \end{aligned} \tag{22}$$

If we now substitute (22) into the governing equations (5), then the terms which are independent of θ in $(5)_1$ and $(5)_3$ give

$$\begin{aligned} &xu_0\frac{\partial u_0}{\partial x} + (w_0 - \tfrac{1}{2}\eta u_0)\frac{\partial u_0}{\partial \eta} - \frac{\partial^2 u_0}{\partial \eta^2} \\ &+ \tfrac{1}{2}\sum_{j=1}^{\infty}\left\{xu_j\frac{\partial u_j}{\partial x} + (w_j - \tfrac{1}{2}\eta u_j)\frac{\partial u_j}{\partial \eta} - jxv_ju_j\right\} = 0\ , \end{aligned} \tag{23}$$

$$x\frac{\partial u_0}{\partial x} - \tfrac{1}{2}\eta\frac{\partial u_0}{\partial \eta} + \frac{\partial w_0}{\partial \eta} = 0\,, \tag{24}$$

respectively. Meanwhile, equating coefficients of $\cos k\theta$ in $(5)_{1,3}$ and $\sin k\theta$ in $(5)_2$, where k is an integer, leads to the following sets of equations for u_k, v_k and w_k, $k \geqslant 1$,

$$\begin{aligned} &x\left(u_0\frac{\partial u_k}{\partial x} + u_k\frac{\partial u_0}{\partial x}\right) + (w_0 - \tfrac{1}{2}\eta u_0)\frac{\partial u_k}{\partial \eta} + (w_k - \tfrac{1}{2}\eta u_k)\frac{\partial u_0}{\partial \eta} - \frac{\partial^2 u_k}{\partial \eta^2} \\ &+ \tfrac{1}{2}\sum_{j=1}^{\infty}\left\{xu_{k+j}\frac{\partial u_j}{\partial x} + (w_{k+j} - \tfrac{1}{2}\eta u_{k+j})\frac{\partial u_j}{\partial \eta} - jxv_{k+j}u_j\right\} \\ &+ \tfrac{1}{2}\sum_{\substack{j=1\\ j\neq k}}^{\infty}\left\{xu_{|k-j|}\frac{\partial u_j}{\partial x} + (w_{|k-j|} - \tfrac{1}{2}\eta u_{|k-j|})\frac{\partial u_j}{\partial \eta} + j\,\mathrm{sgn}(k-j)xv_{|k-j|}y_j\right\} = 0\,, \end{aligned} \tag{25}$$

$$\begin{aligned} &xu_0\frac{\partial v_k}{\partial x} + (w_0 - \tfrac{1}{2}\eta u_0)\frac{\partial v_k}{\partial \eta} - \frac{\partial^2 v_k}{\partial \eta^2} - 2x\delta_{2k} \\ &+ \tfrac{1}{2}\sum_{j=1}^{\infty}\left\{xu_{j+k}\frac{\partial v_j}{\partial x} + (w_{j+k} - \tfrac{1}{2}\eta u_{j+k})\frac{\partial v_j}{\partial \eta} + (k+j)xv_{j+k}v_j\right\} \\ &+ \tfrac{1}{2}\sum_{\substack{j=1\\ j\neq k}}^{\infty}\left\{xu_{|k-j|}\frac{\partial v_j}{\partial x} + (w_{|k-j|} - \tfrac{1}{2}\eta u_{|k-j|})\frac{\partial v_j}{\partial \eta} + |k-j|v_{|k-j|}v_j\right\} = 0\,, \end{aligned} \tag{26}$$

where δ_{ij} is the Kronecker delta, and

$$x\frac{\partial u_k}{\partial x} - \tfrac{1}{2}\eta\frac{\partial u_k}{\partial \eta} + \frac{\partial w_k}{\partial \eta} + kxv_k = 0\,. \tag{27}$$

The boundary conditions (6) and (8) now require

$$\begin{aligned} &u_k = v_k = w_k = 0 \quad \text{on} \quad \eta = 0\,, \quad x > 0\,, \quad k \geqslant 0\,; \\ &u_0 \to 1, u_1 \to 0\,, \quad v_1 \to 2, u_k, v_k \to 0 \quad \text{as} \quad \eta \to \infty\,, \quad x > 0\,, \quad k > 1\,; \\ &u_0 = u_b(\eta), v_1 = 2u_b(\eta)\,, \quad u_1 = u_k = v_k = 0 \quad \text{at} \quad x = 0\,, \quad k > 1\,. \end{aligned} \tag{28}$$

To solve equations (23) to (27) we again use a discretization, in this case with both x and η derivatives represented by central differences. The continuity equations (24) and (27) are evaluated at $(i + \frac{1}{2}, j - \frac{1}{2})$, denoted by + in Fig. 3, whilst the momentum equations (23), (25) and (26) are evaluated at $(i + \frac{1}{2}, j)$, denoted by □ in Fig. 3. Each of the series in (22) is truncated at $n = N$, and the discretization procedure described above results in a total of $3N + 2$ non-linear algebraic equations for the unknown quantities u_0, w_0, u_k, v_k, w_k, $1 \leqslant k \leqslant N$. Whilst, in principle, these $3N + 2$ equations may be solved simultaneously using Newton's method, we have chosen to use an iterative method, not dissimilar to that employed in the finite-difference method of Section 4.1, as follows. To determine the solution at station $i + 1$ the unknowns are first estimated from previous stations by extrapolation or, when $i = 1$, by simply taking the initial solution as the estimate. The non-linear equation (23) is then solved for u_0 using Newton's method, which is equivalent to our formal quasi-linearization in Section 4.1, with the linear equations (24) for w_0 and (25),

(26) and (27) for u_k, v_k and w_k $(1 \leqslant k \leqslant N)$ being solved consecutively. In these equations all coefficients and 'forcing' terms are evaluated using the most recently updated values. As with the method described in Section 4.1 the coefficient matrix is tridiagonal, and can be efficiently inverted, the major computational task in this method is evaluating the summations in (23), (25) and (26). Iterative sweeps are made through equations (23)–(27) until the solutions for u_0, w_0, u_k, v_k, w_k $(1 \leqslant k \leqslant N)$ are deemed to have converged according to some pre-set criterion.

This spectral method, perhaps more properly described as a hybrid method, overcomes the difficulty we have highlighted with the finite-difference method and, with reference to Fig. 1, enables us to determine the solution, for all θ, beyond the point S_1, as long as the solution remains regular everywhere. However, as we shall see in the next section, the solution develops a singularity at a finite value of x, say x_s, beyond which the method of this subsection cannot penetrate. Beyond x_s the solution may be developed, in $\theta < \theta_l$, using the finite-difference method of Section 4.1, to yield valuable information in the region $x > x_s$.

5. Results

We begin our discussion of the properties of the three-dimensional boundary-layer flow with results obtained from the spectral method described in Section 4.2. The integration commences at $x = 0$ where we have $u = u_b(\eta)$, $v = 2u_b(\eta)\sin\theta$. We choose $\eta_\infty = 10$ which has proved an adequate representation of the outer edge of the boundary layer where we insist that $|\partial u/\partial y| + |\partial v/\partial y| < 10^{-4}$ throughout our calculations. The step lengths $\delta\eta = 0.1$, $\delta x = 10^{-3}$ were fixed and the number of terms in the series representation taken as $N = 16$ initially. More terms may be added in order to maintain a given degree of accuracy, which is monitored by inspection of the magnitude of the last term of each series. Specifically we have required that $\max\{u_N, v_N, w_N\} < \varepsilon_1$ where $\varepsilon_1 = 10^{-5}$ up to $x = 0.395$, at which point $N = 256$. This value of N was fixed up to $x = 0.401$, which implied $\varepsilon_1 = 5 \times 10^{-3}$, whilst for the last step N was increased to $N = 300$ in order to maintain this order of accuracy.

In Figs. 5 and 6, respectively, we show the development of the shear stress components $\partial u/\partial y|_{y=0}$ and $\partial v/\partial y|_{y=0}$. The streamwise component remains positive as might be expected

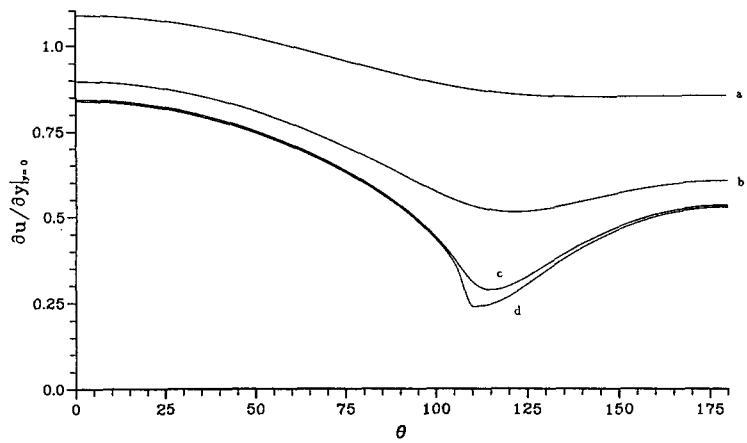

Fig. 5. The variation of $\partial u/\partial y|_{y=0}$ as a function of θ for various values of x: x = (a) 0.125, (b) 0.250, (c) 0.375, (d) 0.402.

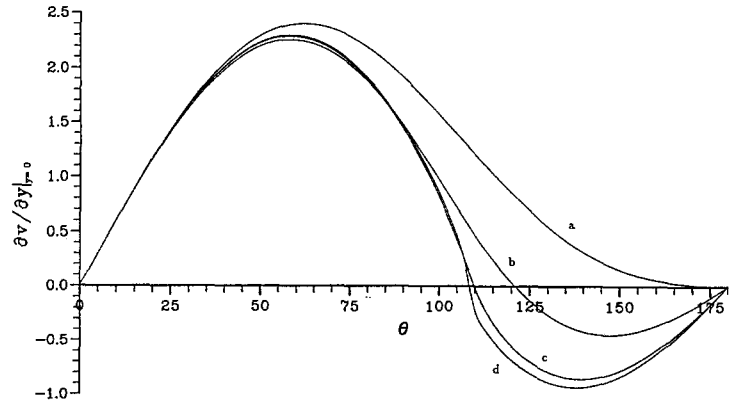

Fig. 6. As Fig. 5 for $\partial v/\partial y|_{y=0}$.

since the cylinder is almost aligned with a uniform flow. However, the transverse component, whilst initially non-negative, eventually changes sign in the neighbourhood of the leeward stagnation line. This is consistent with the results shown in Fig. 2, and we confirm that the point S_1, and the curve $\theta = \theta_l(x)$ on which $\partial v/\partial y|_{y=0}$ vanishes, is in no way exceptional.

Evidence for singular behaviour is provided in Fig. 7 which shows the development of the viscous displacement velocity $w_d(x, \theta)$. This displacement velocity is defined as

$$w_d = \lim_{\eta \to \infty} \{x^{-1/2}(w + 2x\eta \cos\theta)\}\,, \tag{29}$$

and is clearly exhibiting singular behaviour. A careful analysis of the structure shown in Fig. 7 shows that $\max(w_d)$ is increasing as $(x_s - x)^{-3/4}$. This is clearly demonstrated in Fig. 8 where $\{\max(w_d)\}^{-4/3}$ is plotted as a function of x, to reveal a linear behaviour as $x \to x_s = 0.4054$. An apparently similar singularity has been encountered by Goldstein and Leib [12]. It is obvious from Fig. 7 that in order to maintain good resolution in θ, as x_s is approached, it is necessary to increase N, the number of terms in the series, as indicated

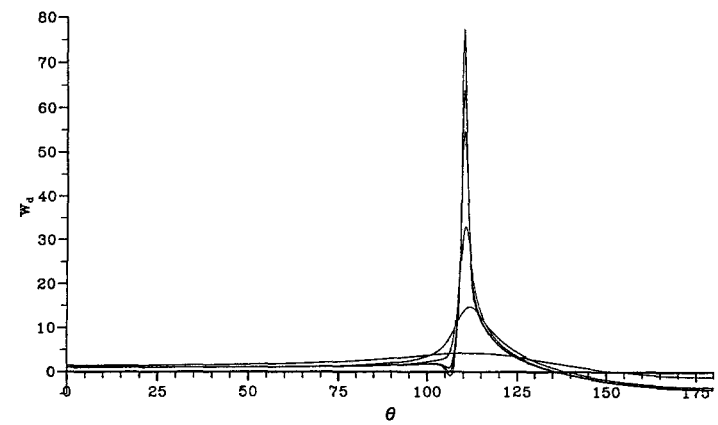

Fig. 7. The variation of the viscous displacement velocity w_d as a function of θ for the x values 0.250, 0.375, 0.395, 0.400, 0.401, 0.402. Increasing x corresponds to increasing $\max(w_d)$.

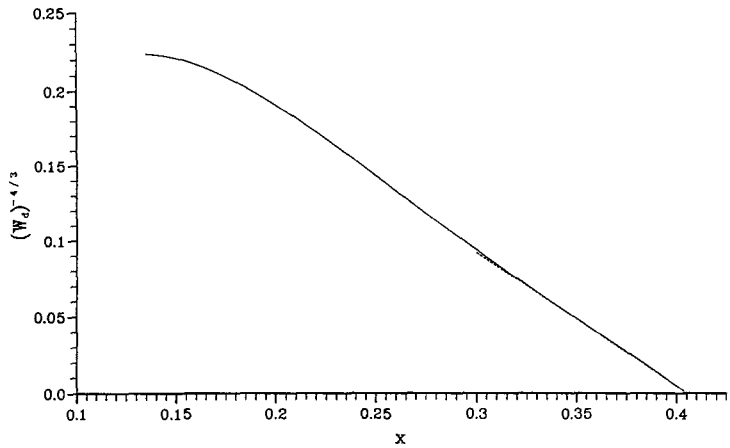

Fig. 8. A plot of $w_d^{-4/3}$ as a function of x. The broken line is a straight line of best fit.

above. It is the displacement velocity that 'drives' the displacement surface. If we represent the latter by $\delta(x, \theta)$ then

$$\frac{\partial \delta}{\partial x} + 2 \sin \theta \frac{\partial \delta}{\partial \theta} = w_d \,, \tag{30}$$

where w_d is given by (29). The solution of this equation is presented in Fig. 9. We note that δ does not appear to be unbounded at the singular point although its θ-derivative is. Such behaviour is consistent with that we have predicted for w_d.

Further evidence for the eruptive nature of the singularity which we have uncovered is given in Fig. 10. There we show the cross-section of the stream-surfaces in the boundary layer in a plane $x =$ constant. These are calculated from the equation

$$\frac{\mathrm{d}y}{\mathrm{d}\theta} = \frac{\bar{w}}{v} \,, \tag{31}$$

and in the figure itself the boundary layer has been magnified by a factor $O(R_e^{1/2})$. Distortion

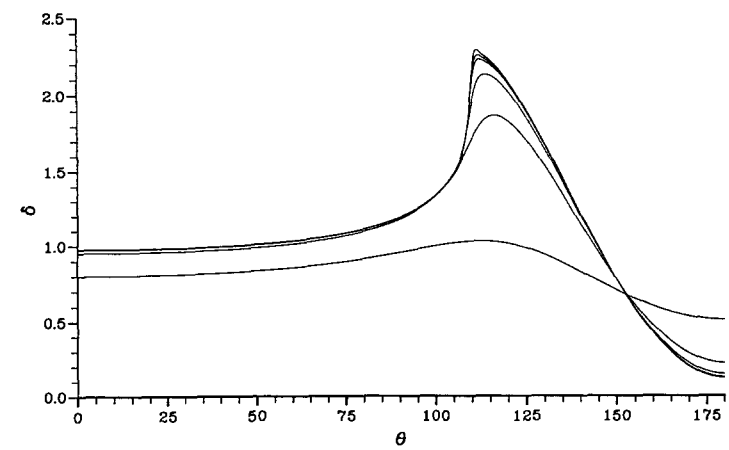

Fig. 9. As Fig. 7 for the displacement surface δ. Increasing x corresponds to increasing max(δ).

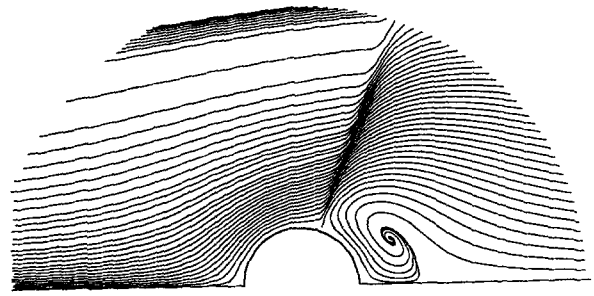

Fig. 10. A cross section of the stream surfaces in the boundary layer, which has been radially magnified by a factor $O(R_e^{1/2})$.

of the cross-flow streamlines in the neighbourhood of $\theta = \theta_l$ reveals the erupting singular behaviour.

From these calculations using our spectral method we show, finally, in Fig. 11 surface streamlines which are calculated from the equation

$$\frac{\mathrm{d}\theta}{\mathrm{d}x} = \left.\frac{\partial v/\partial y}{\partial u/\partial y}\right|_{y=0}. \tag{32}$$

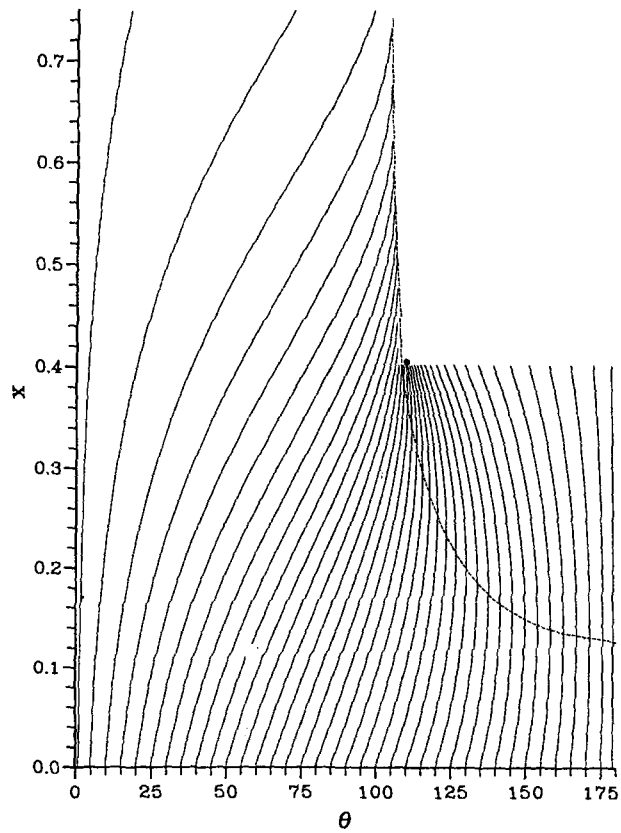

Fig. 11. Surface streamlines for $0 \leq \theta \leq \pi$ calculated from equation (30). The broken line represents the curve S_1S_2 of Fig. 1. The initial singularity is shown as •.

Included in the figure is the line $\theta = \theta_l(x)$ shown in Fig. 1 as S_1S_2. As x_s is approached the surface streamlines converge onto the singular point, which is to be expected if fluid is to be provided to supply the massive outflow depicted in Fig. 7. The singular point itself lies close to but not on the curve $\theta = \theta_l(x)$ and our best estimate of its position is at the point $x_s = 0.4054$, $\theta_s = 110.1°$. We note that neither component of skin friction vanishes at this point.

As we have already remarked, the appearance of a singularity in the solution of equations (5) precludes the possibility of our continuing the solution beyond $x = x_s$ using the spectral method. However, Fig. 11 shows that the solution has been continued into the region $x > x_s$, $\theta < \theta_l$. This continuation has been achieved by employing the finite-difference method of Section 4.1, with initial data provided from the solution at $x = 0.4$. To maintain the high accuracy that characterizes our solution for $x < x_s$, we have taken $\delta x = 10^{-4}$, $\delta\theta = \pi/7200$. The solution calculated by this method in $x > x_s$ terminates in a line $\theta = \theta_{ls}(x)$ at which both components of shear stress $\partial u/\partial y$, $\partial v/\partial y$, at $y = 0$, exhibit singular behaviour in the sense that their θ-derivatives are unbounded. Neither component vanishes at this line but it appears the component of shear stress normal to it does. The lines $\theta = \theta_l$ and $\theta = \theta_{ls}$ are almost coincident, and almost coincident with a generator of the cylinder. The singularity in the shear stress is of a square-root nature, so that beyond x_s our solution terminates in a line of singularities of the Goldstein type. A further discussion of the structure of the solution in the neighbourhood of this line is given in Appendix A. In Figs. 12 and 13 we show the components $\partial u/\partial y|_{y=0}$ and $\partial v/\partial y|_{y=0}$ at various stations. The developing singularity, as $\theta \to \theta_{ls}$ is in evidence, but also it is clear that the solution is virtually independent of x in this region. From our solution we have estimated the singular line $\theta = \theta_{ls}(x)$ and this is shown in Fig. 14 together with the line $\theta = \theta_l(x)$. For two-dimensional steady flow past a circular cylinder the boundary-layer solution fails in the manner of a Goldstein singularity at $\theta = \theta_g = 104.4°$. This quantity is also shown in Fig. 14 and appears to be an asymptote for the curves θ_l and θ_{ls}. We may conclude that beyond the point at which the three-dimensional boundary-layer solution fails the attached boundary layer, that is for $\theta < \theta_{ls}$, is virtually independent of the streamwise coordinate x. For $\theta > \theta_{ls}$ this cannot be the case, and we

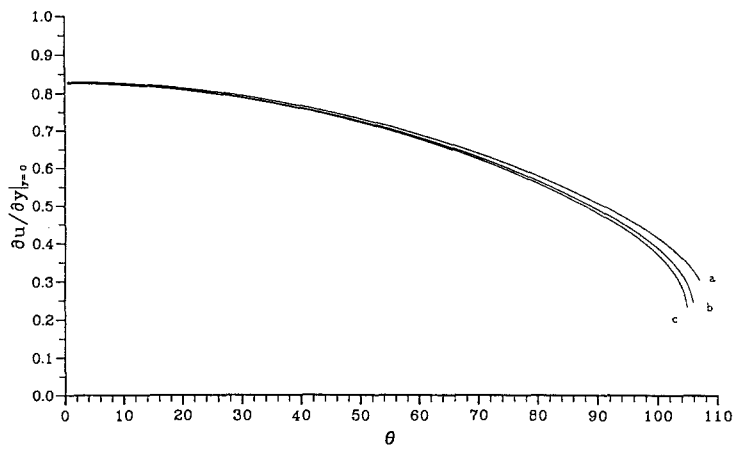

Fig. 12. As Fig. 5 but with (a) $x = 0.45$, (b) $x = 0.55$, (c) $x = 0.65$. For $x > 0.65$ the curves are almost indistinguishable.

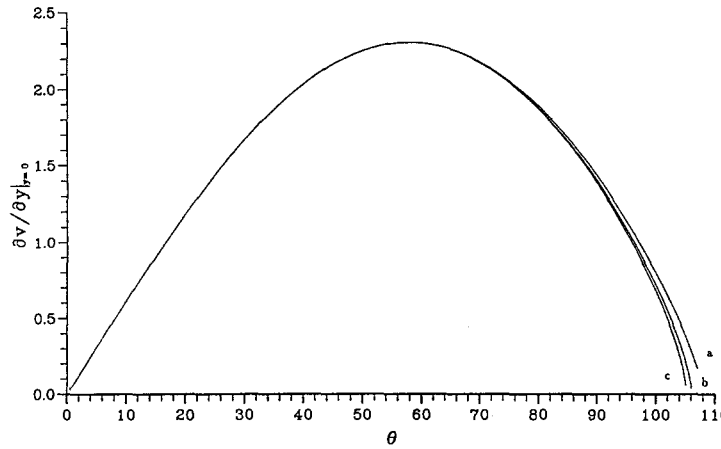

Fig. 13. As Fig. 6 but with (a) $x = 0.45$, (b) $x = 0.55$, (c) $x = 0.65$. For $x > 0.65$ the curves are virtually indistinguishable.

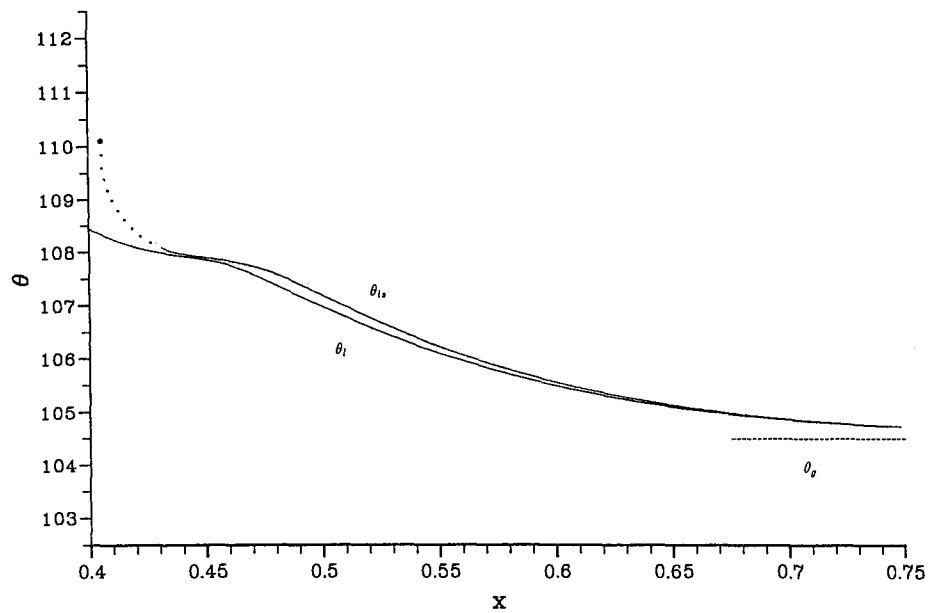

Fig. 14. The variation with x of θ_l and θ_{ls}. The broken line shows the position of the Goldstein singularity in two-dimensional flow, the initial singular point is denoted by •.

expect a growing wake region to continue its development in the manner suggested by our analysis of Section 3 on the leeward generator.

6. Conclusions

A three-dimensional boundary-layer calculation on a yawed body of revolution has provided a fundamental insight into boundary-layer separation of 'open' type. In particular it has been shown that the solution on a cylinder of circular cross-section, at small angles of yaw, develops a singularity at a point, that we interpret as the point at which the flow first erupts

from the boundary layer to form a streamwise vortex configuration. There is an analogy between the flow under consideration, and the unsteady flow when an infinite cylinder moves impulsively in a direction perpendicular to its generators. The analogy would be complete if, in equation $(3)_2$, the convective velocity $u \equiv 1$, in which case the singular behaviour would require $\max(w_d) \sim (x_s - x)^{-7/4}$ as $x \to x_s$. However, as we have seen, $(x_s - x)^{-3/4}$ is the appropriate singular behaviour in the three-dimensional case that has been obtained. Beyond this initial singular breakdown the solution of the boundary-layer equations continues to fail along a line, almost coincident with a generator of the cylinder, perpendicular to which the surface shear stress vanishes. This stress component vanishes with a square-root singular behaviour, and so the line along which the solution fails is essentially a line of Goldstein singularities. As noted by Cousteix [13] the appearance of a line of singularities in a three-dimensional boundary layer calculation is not unknown. Our calculations are consistent with the reasonable hypothesis that this singular line is asymptotic to the generator of the cylinder at which the boundary-layer solution fails in two-dimensional flow. A major conclusion of this investigation is, therefore, that separation of 'open' type on a body of revolution is characterized by a line of singularities of the boundary layer solution. This appears to contradict the views of Maskell [14] (see Crabtree et al. [15]) that such a separation line will be a line of ordinary points. A further conclusion concerns the development of the solution beyond the point $x = x_s$ of the initial breakdown. There it has been shown that between the line of attachment on the windward stagnation line, and the line of separation characterized by Goldstein singularities, the flow conditions are virtually independent of distance measured along the cylinder.This provides some basis for the so-called 'independence principle' that has been widely adopted for yawed configurations.

Finally, we acknowledge that the appearance of singularities of the type under discussion are an artefact of an imposed outer flow, and may lead to only an approximate representation of a high Reynolds number flow. A possible resolution of this difficulty may be found in a viscous/inviscid interactive approach.

Acknowledgement

This work was carried out under a research agreement between the University of East Anglia and the Department of Trade and Industry, monitored by the Aerodynamics and Propulsion Department of the Defence Research Agency's Aerospace Division, Farnborough.

Appendix A

Conditions at the separation line

In this appendix we model the conditions at the separation line which, as we have seen in Section 5, is characterized as a line of singularities of the type discussed by Goldstein for two-dimensional flow. The line is almost a straight line, coincident with a generator of the cylinder. Along this there is a favourable pressure gradient in the direction of x increasing, whilst perpendicular to it, in the direction of θ increasing, the pressure gradient is adverse.

For simplicity we assume that the separation line is a straight line, $\theta = \theta_s$, and at a point (x_0, θ_s) on it the pressure is given by

$$p = \text{const.} - p_0(x - x_0) + p_1(\theta - \theta_s) + \cdots \tag{33}$$

where the constants p_0, $p_1 > 0$. At the separation line the shear stress component perpendicular to it vanishes, but the component along it does not. So, at (x_0, θ_s), we have

$$\begin{aligned} v &= \tfrac{1}{2}a_2 y^2 + a_4 y^4 + \cdots , \\ u &= b_1 y + \tfrac{1}{2}b_2 y^2 + b_4 y^4 + \cdots , \end{aligned} \tag{34}$$

where the coefficients a_i, b_i are, in general, functions of x, evaluated at $x = x_0$ in (34). If we now introduce the new variables

$$\theta_1 = (\theta_s - \theta)^{1/4} , \qquad \eta_1 = \frac{y}{\sqrt{2}\theta_1} , \tag{35}$$

and write

$$\begin{aligned} u &= \sqrt{2}b_1\theta_1\eta_1 + 2\theta_1^2\bar{U} , \\ v &= 2\theta_1^2\bar{V} , \\ \bar{w} &= \frac{\bar{W}}{\sqrt{2}\theta_1} , \end{aligned} \tag{36}$$

then the boundary-layer equations (3), in which the pressure gradient is calculated from (33), and not neglected in $(3)_1$, become, with $\dot{b}_1 = \mathrm{d}b_1/\mathrm{d}x$,

$$\begin{aligned} &\theta_1^2(\sqrt{2}b_1\eta_1 + 2\theta_1\bar{U})\left(\sqrt{2}\dot{b}_1\eta_1 + 2\theta_1\frac{\partial\bar{U}}{\partial x}\right) + \bar{V}\left(\eta_1\frac{\partial\bar{U}}{\partial\eta_1} - 2\bar{U} - \theta_1\frac{\partial\bar{U}}{\partial\theta_1}\right) + \bar{W}\left(\frac{b_1}{\sqrt{2}\theta_1} + \frac{\partial\bar{U}}{\partial\eta_1}\right) \\ &\quad = p_0 + \cdots + \frac{\partial^2\bar{U}}{\partial\eta_1^2} , \end{aligned} \tag{37}$$

$$2\theta_1^3(\sqrt{2}b_1\eta_1 + 2\theta_1\bar{U})\frac{\partial\bar{V}}{\partial x} + \bar{V}\left(\eta_1\frac{\partial\bar{V}}{\partial\eta_1} - 2\bar{V} - \theta_1\frac{\partial\bar{V}}{\partial\theta_1}\right) + \bar{W}\frac{\partial\bar{V}}{\partial\eta_1} = -p_1 + \cdots + \frac{\partial^2\bar{V}}{\partial\eta_1^2} , \tag{38}$$

$$2\sqrt{2}\dot{b}_1\theta_1^3\eta_1 + 4\theta_1^4\frac{\partial\bar{U}}{\partial x} + \eta_1\frac{\partial\bar{V}}{\partial\eta_1} - 2\bar{V} - \theta_1\frac{\partial\bar{V}}{\partial\theta_1} + \frac{\partial\bar{W}}{\partial\eta_1} = 0 . \tag{39}$$

We now expand the reduced velocity components (36) as,

$$\begin{aligned} \bar{U} &= u_0 g_0'(\eta_1) + \theta_1 u_1 g_1'(\eta_1) + \theta_1^2 u_2 g_2'(\eta_1) + \cdots , \\ \bar{V} &= v_0 f_0'(\eta_1) + \theta_1 v_1 f_1'(\eta_1) + \theta_1^2 v_2 f_2'(\eta_1) + \cdots , \\ \bar{W} &= v_0(3f_0 - \eta_1 f_0') + v_1\theta_1(4f_1 - \eta_1 f_1') + v_2\theta_1^2(5f_2 - \eta_1 f_2') + \cdots , \end{aligned} \tag{40}$$

where a prime denotes differentiation with respect to η_1, and u_i, v_i are constants.

If we now introduce (40) into (38) we have, at $O(1)$,

$$f_0''' - 3v_0 f_0 f_0'' + 2v_0 f_0' = p_1 ,$$

with solution that satisfies the no-slip condition at $\eta_1 = 0$, and matches with $(34)_1$,

$$f_0 = \frac{p_1}{6v_0}\eta_1^3 , \tag{41}$$

provided that $a_2 = p_1$. The terms $O(\theta_1)$ in (38) now give, as equation for f_1,

$$f_1''' - v_0(\eta_1 f_0' f_1'' - 5f_0' f_1' + 4f_0'' f_1) = 0 ,$$

which, with f_0 given by (41), has the solution satisfying no-slip

$$f_1 = \alpha_1 \eta_1^2 , \tag{42}$$

where α_1 is a constant which will depend, in particular, upon conditions for $\theta < \theta_s$.

The results obtained so far, perhaps unsurprisingly, indicate that two-dimensional effects dominate. Consider next equation (37). The terms at $O(1)$ yield

$$g_0''' + \tfrac{1}{2}p_1\eta_1^2(2g_0' - \eta_1 g_0'') = -\frac{p_0}{u_0} + \frac{\sqrt{2}b_1 v_1 \alpha_1}{u_0}\eta_1^2 ,$$

the solution of which, that satisfies no-slip and matches with $(34)_2$, is

$$g_0 = -\frac{p_0}{6u_0}\eta_1^3 + \sum_{n=0}^{\infty} \delta_n \eta_1^{4n+5} , \tag{43}$$

provided that $b_2 = -p_0$. In order to determine g_1, we must first know f_2. This is, again, given by the corresponding two-dimensional result, since (38) clearly shows that only at $O(\theta_1^3)$ do we deviate from that, which is

$$f_2 = \alpha_2 \eta_1^2 - \tfrac{1}{15}\alpha_1^2 \eta_1 ,$$

where α_2 is a second arbitrary constant that depends upon conditions away from the separation line. The terms $O(\theta_1)$ in (37) now give, for g_1,

$$g_1''' - \tfrac{1}{2}p_1(\eta_1^3 g_1'' - 3\eta_1^2 g_1') = \frac{3v_2 b_1 \alpha_2}{\sqrt{2}u_1}\eta_1^2 - \frac{2v_1 \alpha_1 p_0}{u_1}\eta_1^3 + \sum_{n=0}^{\infty}\{\beta_n \eta_1 + \gamma_n\}\eta_1^{4n+5} ,$$

where the constants β_n, γ_n are given in terms of the known constants δ_n of (43). The solution of this equation for g_1, which satisfies no-slip, is

$$g_1 = -\frac{v_1 \alpha_1 p_0}{u_1 p_1}\eta_1^2 + \sum_{n=0}^{\infty}\{\bar{\beta}_n + \bar{\gamma}_n \eta_1^3\}\eta_1^{4n+5} , \tag{44}$$

where the constants $\bar{\beta}_n$, $\bar{\gamma}_n$ are known.

Now, the leading term of (44) will contribute, to u in $(34)_2$, a term

$$-\frac{2\sqrt{2}v_1 \alpha_1 p_0}{p_1}\theta_1^2 y ,$$

first as f_1 contributes a term $O(\theta_1^2 y)$ to v. So, we may conclude that the square-root singularity which appears in the transverse component of shear stress is also present in the longitudinal component provided both α_1 and p_0 are non-zero.

References

1. S. Goldstein, On laminar boundary-layer flow near a position of separation. *Quart. J. Mech. appl. Math.* 1 (1948) 43–69.
2. K. Stewartson, On Goldstein's theory of laminar separation. *Quart. J. Mech. appl. Math.* 11 (1958) 399–410.
3. R.M. Terrill, Laminar boundary-layer flow near separation with and without suction. *Phil. Trans. R. Soc.* A253 (1960) 55–100.
4. K. Stewartson, Multistructured boundary layers on flat plates and related bodies. *Adv. appl. Mech.* 14 (1974) 145–239.
5. F.T. Smith, On the high Reynolds number theory of laminar flows. *IMA J. appl. Math.* 28 (1982) 207–281.
6. S.N. Brown, Singularities associated with separating boundary layers. *Phil. Trans. R. Soc.* A257 (1965) 409–444.
7. J.C. Cooke, The laminar boundary layer on an inclined cone. ARC R & M No. 3530 (1965).
8. M.J. Lighthill, Introduction. Boundary layer theory. In: L. Rosenhead (ed.), *Laminar Boundary Layers*, Clarendon Press Oxford (1963) Chap 2.
9. L.L. van Dommelen and S.F. Shen, The spontaneous generation of the singularity in a separating boundary layer. *J. Comp. Phys.* 38 (1980) 125–140.
10. S.J. Cowley, Computer extension and analytic continuation of Blasius' expansion for an impulsive flow past a circular cylinder. *J. Fluid Mech.* 135 (1983) 389–405.
11. I. Proudman and K. Johnson, Boundary-layer growth near a rear stagnation point. *J. Fluid Mech.* 12 (1962) 161–168.
12. J. Cousteix, Three-dimensional and unsteady boundary-layer computations. *Ann. Rev. Fluid Mech.* 18, (1986) 173–196.
13. M.E. Goldstein and S.J. Leib, Three-dimensional boundary-layer instability and separation induced by small-amplitude streamwise vorticity in the upstream. *J. Fluid Mech.* 246 (1993) 21–41.
14. E.C. Maskell, Flow separation in three dimensions. *Rep. Aero. Res. Coun. Lond.* No. 18063 (1955).
15. L.F. Crabtree, D. Küchemann and L. Sowerby, Three-dimensional boundary layers. In: L. Rosenhead (ed.), *Laminar Boundary Layers*. Clarendon Press Oxford (1963) Chap. 8.